Light Induced Processes in $CsPbBr_3$–Au Hybrid Nanocrystals: Electron Transfer and Expulsion of Au

Jishnudas Chakkamalayath,[1,2] Gregory V. Hartland[1,2*] and Prashant V. Kamat[1,2,3*]

[1]Radiation Laboratory, [2]Department of Chemistry and Biochemistry, and [3]Department of Chemical and Biomolecular Engineering.

University of Notre Dame, Notre Dame, Indiana 46556, United States

Abstract

Semiconductor-metal heterostructures such as $CsPbBr_3$–Au are useful in photocatalysis. When Au nanoparticles are deposited on the $CsPbBr_3$ nanocrystal surface they efficiently quench the photoluminescence of the semiconductor. This process has been studied by femtosecond transient absorption spectroscopy measurements, which indicate that electron transfer to the Au nanoparticles occurs from both hot and relaxed electrons in the conduction band of $CsPbBr_3$. The electron transfer rate constant is much larger for the hot electrons compared to the relaxed electrons. Under steady state photoirradiation of $CsPbBr_3$–Au heterostructure, the photogenerated electrons from the excited $CsPbBr_3$ nanocrystals continue to charge the Au nanoparticles. After sufficient irradiation, the gold nanoparticles dissociate from the $CsPbBr_3$ surface and aggregate into larger size gold nanoparticles. The expulsion of gold nanoparticles restores the original luminescence behavior of $CsPbBr_3$ nanocrystals. The spectroscopic and morphological studies provide insight into the expulsion of gold nanoparticles in photoirradiated $CsPbBr_3$ –Au heterostructures.

TOC Graphics

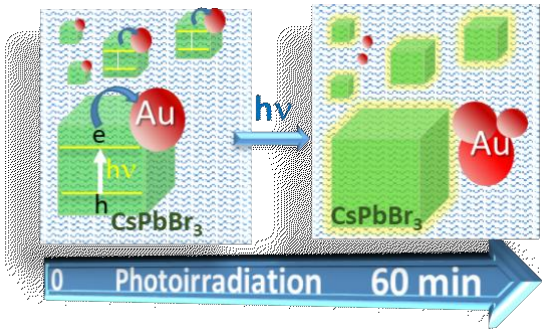

Introduction

Semiconductor-metal heterostructures are widely used in photocatalytic water splitting and other chemical transformations.[1-3] The presence of a noble metal (e.g. Au) at the semiconductor surface can quickly capture the photogenerated electrons and thus facilitates overall charge separation.[4] The photocatalytic performance of such a noble metal-modified semiconductor can lower the overpotential for reduction of H^+ ions. While recent focus involving gold nanoparticles has centered around plasmonic catalysis or hot electron transfer, they are inherently good electron acceptors and promote reduction processes.[5-13] The electron storage and transfer properties of gold nanoparticles can be realized through nonplasmonic (<3 nm) Au nanoparticles. Electron storage in small Au nanoparticles has been demonstrated through quantized capacitance measurements.[14,15] Blue-shifts in the plasmon band of the metal nanoparticles during photoirradiation of semiconductor-metal heterostructures, such as TiO_2-Ag or TiO_2-Au, have also been used to demonstrate electron transfer from the semiconductor to the metal.[16-18]

The emergence of $CsPbBr_3$ nanocrystals, a nanoscale metal halide perovskite system with high luminescent and favorable charge transfer properties offers new opportunities to explore applications of perovskites in photocatalysis.[19-21] The ability to tune their bandgap through halide composition makes these materials potential candidates for the development of solar cells,[22-25] light emitting devices[26,27] and high energy detectors.[28-31] Plasmonic gold nanoparticles have been employed to boost the performance of perovskite solar cells. [32-34] However, the diffusion of gold from the metal contact in a solar cell has been found to deteriorate the solar cell performance.[35,36]

Halide perovskites are inherently unstable in polar solvents. Although efforts have been made to design core@shell heterostructures such as $CsPbBr_3$@ZnS[37] and $CsPbBr_3$@CdS[38] to improve their stability in polar solvents, their application in photocatalysis remain limited. Another difficulty in designing perovskite photocatalyst is the synthesis of $CsPbBr_3$-metal heterostructure with a controllable morphology. In our earlier study, we showed that addition of small amounts of $AuBr_4^-$ resulted in the formation of nanometer sized gold nanoparticles.[39] If we increase the concentration of $AuBr_4^-$ to grow larger size plasmonic Au nanoparticles, one sees substitution of Pb^{2+} with Au^{3+} to form $Cs_2Au_2Br_6$.[40] This substitution is driven by the concentration of metal ions and can be readily suppressed in the presence of excess Pb^{2+} ions. Thus, the design of a stable and tunable perovskite-metal heterostructures is a complicated process that remains a major challenge in perovskite photocatalysis.

The obvious question then is why it is so difficult to design a perovskite-metal nanoassembly that can be directly employed in a photocatalysis process. This paper addresses this issue through studies of $CsPbBr_3$-Au heterostructures. Spectroscopic and morphological changes following bandgap excitation of the $CsPbBr_3$ moiety have been examined. The results show fast electron transfer from $CsPbBr_3$ to Au, and subsequent photoinduced expulsion of the Au nanoparticles from the $CsPbBr_3$–Au heterostructures.

Experimental Section

Chemicals. Cesium carbonate (Cs_2CO_3, 99.9%, Sigma Aldrich), Lead (II) bromide ($PbBr_2$, 99.99%, Sigma Aldrich), Oleic acid (OLA, 90%, Sigma Aldrich), Oleylamine (OLAm, technical grade 70%, Sigma Aldrich), 1-Octadecene (ODE, technical grade 90%, Sigma Aldrich), Methyl acetate (MeOAc, 99.98%, Gold(III) bromide ($AuBr_3$, 99.99%, Sigma Aldrich), Toluene (Anhydrous, 99.99%, Sigma Aldrich, Ethanol (200 proof, Koptec).

Synthesis of $CsPbBr_3$ nanocrystals (NCs). $CsPbBr_3$ NCs were synthesized following a modified procedure adapted from Protesescu et al.[41] Cs-oleate was prepared by mixing 0.153 g of Cs_2CO_3, 1.4 mL of OLA, and 3 mL of ODE in a 25 mL round bottom flask. The mixture was degassed at 80 °C for 1 hour. The lead bromide precursor was prepared by adding 3 mL of OLA, 3 mL of ODE, and 0.414 g of $PbBr_2$ to a 25 mL round bottom flask and degassing for 1 hour at 80 °C. After one hour, the temperature was raised to 170 °C, and 1.5 mL of OLAm was added to the mixture. The solution was degassed for one more minute. The vacuum was then turned off, and the flask was put into a nitrogen environment. Simultaneously, the Cs-oleate precursor was brought up to 120 °C and put under a nitrogen atmosphere. Once both solutions have reached the target temperatures, 2mL of the Cs-oleate solution was injected into the lead-bromide precursor with a heated syringe (from the oven). The mixture was then immediately put in an ice bath until it reached a temperature of 65 °C.

The nanocrystals were washed with approximately 20 mL of 1-Octadecene and transferred to a 50 mL centrifuge tube. This was then spun down for 10 minutes at 7800 rpm. The supernatant was discarded, and the pellet was washed with 5 mL of ODE. The nanocrystals were again centrifuged for 10 minutes at 7800 rpm. The pellet was dispersed in 5 mL toluene and washed with 5 mL of methyl acetate. The nanocrystals were spun down again for 10 minutes at 7800 rpm. The supernatant was discarded, and the pellet was dispersed in 3 mL toluene and again centrifuged for 10 minutes at 7800 rpm. The supernatant was collected and preserved for further experiments.

Synthesis of Au-$CsPbBr_3$ hybrid nanocrystals. $AuBr_3$ was dissolved in 1:10 v/v ethanol/toluene mixture to get 5.15 mM solution. 10 µL OLA was added to 1 mL of 5.15 mM $AuBr_3$ solution and the solution was never stored for longer than an hour.[40] The prepared $AuBr_3$ solution was swiftly added to $CsPbBr_3$ nanocrystals in toluene to get the hybrid nanocrystals. The stability of $CsPbBr_3$ in 0.1 and 0.4% ethanol containing toluene was checked by monitoring absorption and emission spectra (Figure S1). It was found to be stable.

Characterization Methods. UV–visible absorption spectra were recorded using a Cary 50 Bio spectrophotometer (Varian). Emission spectra were collected using a Horiba Jobin Yvon Fluorolog-3 spectrophotometer. The photoluminescence decay of the samples was monitored and recorded by time-correlated single-photon counting (TCSPC) using a Horiba Jobin Yvon system with a IBH DataStation Hub for timing with a 371nm nano LED light source. Transmission electron microscopy (TEM) and Scanning Transmission Electron Microscopy (STEM) imaging were carried out using FEI Titan 80-300 (300 kV) high-resolution transmission electron microscope. X-ray diffraction (XRD) analysis was performed by using D8 Advance Davinci, Bruker X-ray diffractometer with Cu Kα X-ray (λ = 1.5406 Å) and for all the samples, the value of 2θ was varied from 10° to 70° with a scan rate of 0.3° min^{-1}. The colloidal suspension of nanocrystals in a quartz cuvette was subjected to 1Sun (100 mW/cm^2) visible light excitation. The absorbance and emission spectra and other spectral characterization were made on samples irradiated at different irradiation times.

Transient Absorption Experiments. Femtosecond transient absorption measurements were carried out using a Spectra-Physics Solstice Ace laser system (800 nm fundamental, ~5 mJ/pulse, fwhm = ~30 fs, repetition rate of 1 kHz) with detection software from Ultrafast Systems (Helios). A small portion of the fundamental beam was frequency-doubled to 400 nm (using a 1 mm thick BBO crystal) to generate the pump beam, and another part of the fundamental beam was passed through an optical delay stage and focused onto a sapphire crystal to generate a white-light continuum probe pulse. The pump and probe

beams are spatially overlapped onto the sample such that the probe is within the area of pump irradiation. The pump beam was sent through an iris of known diameter and the power was adjusted via a neutral density filter wheel to keep the power density at ~15 μJ/cm^2 for these experiments. Under these conditions the transient absorption experiments do not show any evidence of multiple exciton/Auger recombination effects. The 2D perovskite films were placed in a custom vacuum cell and pumped down/refilled with argon 3x before measurement, to eliminate any potential interactions with oxygen.

Results and Discussion

$CsPbBr_3$ nanocrystals and $CsPbBr_3$-Au Heterostructures. The $CsPbBr_3$ nanocrystal suspension stabilized with oleylamine/oleic acid ligands was prepared as per the literature procedure.[41] Spectrum *a* in Figure 1A shows the absorption characteristics of $CsPbBr_3$ nanocrystals with an excitonic peak at 500 nm. Addition of $AuBr_4^-$ to this solution results in the formation of Au nanoparticles on the surface of the

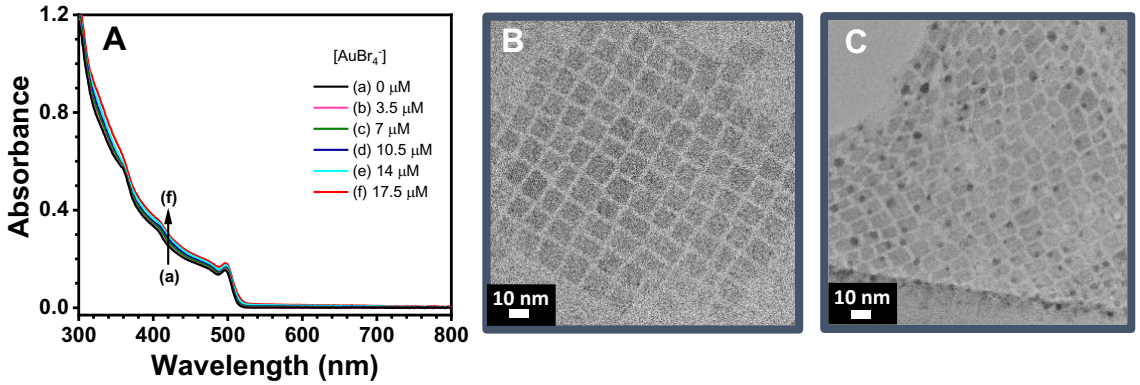

Figure 1: (A) Absorption spectra of $CsPbBr_3$ nanocrystals containing 0 to 17.5 μM of $AuBr_4^-$ in toluene. Representative example of TEM images of (B) $CsPbBr_3$ and (C) Au-$CsPbBr_3$ nanoparticles. The histogram analysis presented in SI show average size of 8.1± 1.1 nm for $CsPbBr_3$ and 8.1± 1.4 nm for $CsPbBr_3$-Au heterostructures. We expect gold nanoparticles to be between 1-2 nm.

perovskite nanocrystals. The amine groups of oleylamine are capable of reducing $AuBr_4^-$ to form small Au nanoparticles.[40,42] Representative TEM images of the $CsPbBr_3$ and $CsPbBr_3$-Au samples are shown in Figure 1. The gold nanoparticles formed on the surface of $CsPbBr_3$ have diameters in the range of 1-2 nm (Figure S2C in the supporting information). Size distribution analysis (Figure S2A and S2B in the suporting information) shows average sizes of the semiconductor moiety of 8.1± 1.1 nm for $CsPbBr_3$ and 8.1± 1.4 nm for $CsPbBr_3$-Au nanocrystals. This shows that there are no major changes in the morphology of the $CsPbBr_3$ nanocrystals upon the deposition of the Au nanoparticles onto their surfaces. Based on the TEM image analysis we expect ~85% of $CsPbBr_3$ particles to have at lease one Au nanoparticle. (Any Au clusters that may be hidden in the background of $CsPbBr_3$ are not included in this coverage) The gold nanoparticles formed on the surface of $CsPbBr_3$ in our experiments are too small to exhibit a plasmon resonance. However, their presence is confirmed through the small increase in the absorption below 500 nm and the TEM measurements (Figure 1C). The XRD pattern of $CsPbBr_3$ and $CsPbBr_3$-Au nanoparticles are shown in

Figure S3. The XRD pattern $CsPbBr_3$-Au shows an additional peak corresponding to Au, thus confirming its presence in the hybrid nanostructure.

It has been shown earlier that Au(III) at higher concentrations can substitute Pb^{2+} to form $Cs_2Au_2Br_6$.[40] This substitution is marked by the strong absorbance in the long wavelength region (500-700 nm). The absence of such absorbance in the long wavelength region indicates that the concentration range of <17.5 μM of $AuBr_4^-$ employed in the present study excludes the possibility of the Au for Pb substitution. One needs to increase the concentration of gold salt to the millimolar range to see such effects.

Tracking Excited State Interactions. The $CsPbBr_3$ nanocrystals are highly luminescent with a quantum efficiency reaching near unity.[43] The bright green emission of $CsPbBr_3$ provides a convenient means to probe excited state interaction with the small gold nanoparticles. The emission spectra of $CsPbBr_3$

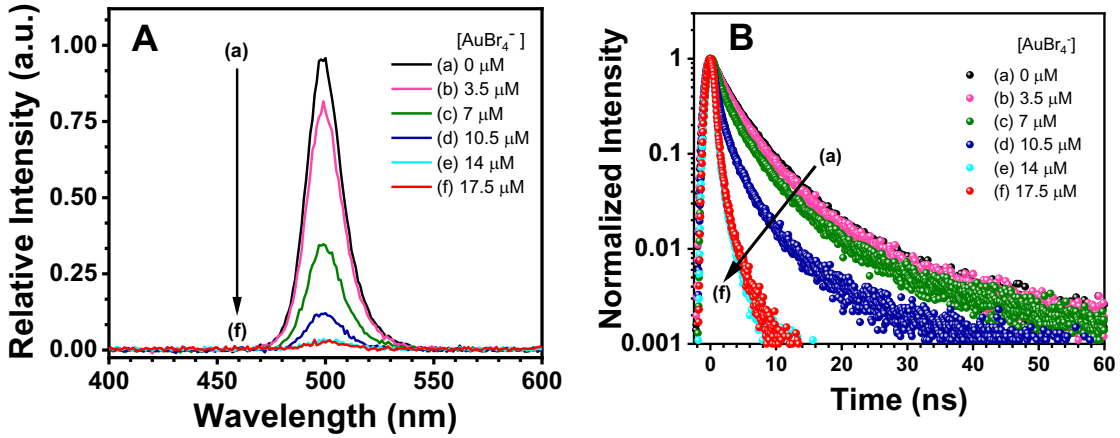

Figure 2: (A) Steady state photoluminescence, PL (Excitation 375 nm) and (B) PL decay (510 nm) of $CsPbBr_3$ nanocrystals and Au-$CsPbBr_3$ heterostructures suspension in toluene recorded at different concentrations of Au (Excitation 370 nm). The average lifetime decreased from 6.9 ns to 1.2 ns.

nanocrystals in toluene are shown in Figure 2A. With increasing concentration of $AuBr_4^-$ we observe quenching of $CsPbBr_3$ emission. Nearly 100% quenching is seen at a concentration of 17.5 μM $AuBr_4^-$. As shown earlier, at these low concentrations $AuBr_4^-$ interacts with the oleylamine to form gold nanoparticles. These gold nanoparticles are homogeneously distributed across different $CsPbBr_3$ nanoparticles, mostly at the corner sites.

The quenching of emission can be understood from the ability of gold nanoparticles to serve as electron acceptors. These nonplasmonic metal nanoparticles have been shown to capture and store electrons from excited semiconductor nanoparticles.[44-46] The excited state deactivation can be understood from reactions 1 and 2.

$$CsPbBr_3 + h\nu \rightarrow CsPbBr_3\,(h—e) \rightarrow CsPbBr_3 + h\nu' \qquad (1)$$

$$CsPbBr_3\,(h—e) + Au \xrightarrow{k_{et}} CsPbBr_3\,(h) + Au\,(e) \qquad (2)$$

As reaction 2 competes with the reaction 1, we see a decreased emission from the $CsPbBr_3$ nanocrystals when Au is added. We also monitored the emission decay of $CsPbBr_3$ at different Au concentrations. Figure 2B shows emission decay recorded at 510 nm using 370 nm pulsed laser excitation. The decay curves were analyzed using a biexponential fit, $I(t) = \sum_{i=1}^{n} A_i \exp(-t/\tau_i)$ The longer component is likely to arise from the $CsPbBr_3$ nanocrystals that may not have a coverage of Au. In fact with increasing Au concentration, this long lifetime component also decreases. The preexponent factors and lifetimes are presented in Table S1. The two lifetimes estimated for the emission decay decreased from 3.1 ± 0.02 ns and 9.7 ± 0.06 ns for pristine $CsPbBr_3$ to 0.3 ± 0.004 ns and 2.9 ± 0.01 ns for $CsPbBr_3$ –Au (corresponding to 17.5 μM Au). The corresponding average lifetime, $\langle\tau\rangle$, decreased from 6.9 ± 0.4 ns to 1.2 ± 0.06 ns. The decreased lifetime with increasing Au concentration supports the electron transfer quenching of excited $CsPbBr_3$ by the gold nanoparticles (reaction 2).

To further assess the kinetics of electron transfer, we carried out femtosecond transient absorption measurements. The transient absorption spectra of $CsPbBr_3$ and $CsPbBr_3$–Au nanocrystal suspensions were recorded at different probe delays using 400 nm laser pulse excitation (Figures 3A&B). The transient spectrum recorded immediately after laser pulse excitation of $CsPbBr_3$ shows intense bleaching of the exciton band, and a small induced-absorption on the red-side of the band. By comparison to other semiconductor nanocrystal systems, the bleach is attributed to state filling and the absorption to photoexcited carrier induced band-shifts.[47,48] The formation of the bleach signal gives information about how quickly the excited charge carriers relax to the bottom of the conduction band/top of the valence band. In contrast, the dynamics of the bleach recovery report on the recombination of electron-hole pairs within the semiconductor nanoparticle, as well as other pathways by which these charge carriers are lost.[47] For example, any electron transfer to the gold nanoparticles from excited $CsPbBr_3$ (reaction 2) would result in faster bleach recovery.

Figures 3 C&D compare the bleach recovery recorded at 510 nm for the $CsPbBr_3$ and $CsPbBr_3$–Au systems on two different times scales. The analysis of the bleach recovery data is presented in Table S2. It is noticeable from these transient absorption traces that both the rise in the bleach signal (Figure 3C) and the bleach recovery (Figure 3D) are faster for $CsPbBr_3$-Au compared to $CsPbBr_3$. The kinetic differences between the $CsPbBr_3$ and $CsPbBr_3$–Au system data are attributed to electron transfer from the $CsPbBr_3$ to the Au. The relatively long timescale bleach-recovery data provides information about electron transfer for electrons relaxed to the bottom of the conduction band, and fast rise time data is sensitive to electron transfer from hot electrons in the $CsPbBr_3$ conduction band (Scheme 1).

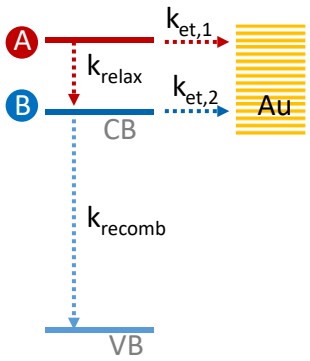

Scheme 1. Kinetic scheme for electron Transfer from photo-excited $CsPbBr_3$ to Au

If we assume electron transfer from excited $CsPbBr_3$ to Au is the only major pathway responsible for faster kinetics, we can estimate a rate constant for electron transfer using the equation (3),

$$k_{et} = 1/\tau_{(CsPbBr_3 - Au)} - 1/\tau_{(CsPbBr_3)} \quad (3)$$

where $\tau_{(CsPbBr_3 - Au)}$ represents the lifetime for the bleach rise (or recovery) of the hybrid nanostructure and $\tau_{(CsPbBr_3)}$ represents the lifetime of the bleach rise (or recovery) of the pristine $CsPbBr_3$ nanocrystals.

In the following, we analyze the bleach recovery and rise time data separately to generate electron transfer rate for the relaxed and hot electrons in the $CsPbBr_3$ conduction band. This approach is justified by the large difference in the time constants for the rise and decay of the bleach signal. Hot electron transfer can occur to either the Au clusters, or to traps at the surface of the particles created by the clusters. These two possibilities cannot be distinguished in the transient absorption experiments. However, the observations of cluster charging and dissociation strongly suggest that electron transfer occur to the clusters. Solution of the coupled rate equations that describe electron transfer and relaxation

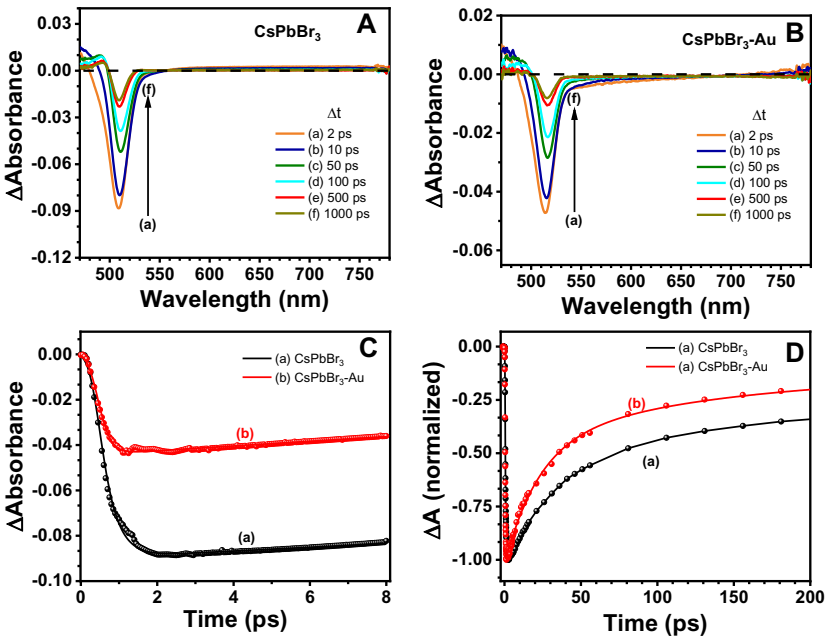

Figure 3: Time-resolved transient absorption (TA) spectra recorded following laser pulse excitation (400 nm) of (A) $CsPbBr_3$ nanocrystals and (B) $CsPbBr_3$-Au heterostructures in deaerated toluene. Bleach growth and recovery recorded at the bleach maximum (510 nm) for $CsPbBr_3$ and Au-$CsPbBr_3$ nanocrystal suspension over (C) 8 ps time scale and (D) a 200 ps timescale (normalized). Points are experimental data and lines are fits to the data.

for the hot and band-edge electrons is presented in the Supporting Information. These simulations confirm that electron transfer to the Au nanoparticles from the hot electrons in the $CsPbBr_3$ conduction band causes a faster rise in the bleach signal.

On the 10 to 200 ps timescale, the bleach recovery time constant decreases from 36.3 ± 0.9 ps for $CsPbBr_3$ to 22.3 ± 1.9 ps for $CsPbBr_3$-Au. Substitution of these lifetimes into Equation (3) gives an electron transfer rate constant, $k_{et,2}$ of $(1.73 \pm 0.27)\times10^{10}$ s^{-1}. This electron transfer rate is consistent with the rate constants observed for other semiconductor-metal systems for electrons relaxed to the bottom of the conduction

band.[49-51] On the few ps timescale the rise time for the bleach signal is 0.35 ± 0.01 ps for $CsPbBr_3$ compared to 0.19 ± 0.01 ps for $CsPbBr_3$-Au. These times constants yield an electron transfer rate constant $k_{et,1}$ of $(2.43 \pm 0.39)x10^{12}$ s^{-1}. The faster rate for electron transfer from the hot electrons compared to the relaxed electrons, and the magnitude of the rate for hot-electron transfer, is again consistent with previous studies of hybrid semiconductor-metal nanostructures.[52-55] Any excess holes left in the $CsPbBr_3$ are scavenged by the surface ligands such as oleylamine.

Effect of Steady-State Irradiation. One of the interesting features of perovskite nanocrystals is their potential in promoting photocatalytic reactions.[20,56-59] The application of $CsPbBr_3$-metal in photocatalysis is yet to be explored fully. In order to assess the long term stability of these materials, we subjected the $CsPbBr_3$ –Au solution to steady state irradiation using 1 Sun white light (100 mW/cm^2). In the absence of Au there is a small change in the absorption and emission spectra (Figure S4). However, the $CsPbBr_3$-Au samples show an interesting behavior. With continued photoirradiation the quenched emission of $CsPbBr_3$ -Au recovers. Figure 4A and B show the emission spectra of $CsPbBr_3$-Au nanoparticle suspension kept in dark and under continuous white light emission. With increasing time we see an enhancement in the emission as we continue the light irradiation for 30 min. Figure 4C shows the photoluminescence recovery following the light irradiation. More than 95% of original photoluminescence was restored

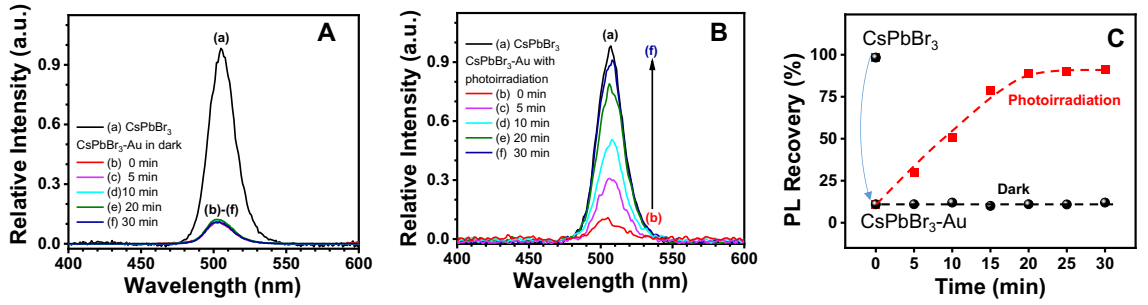

Figure 4: Photoluminescence spectra (Excitation 375 nm) of $CsPbBr_3$ (spectrum a) and $CsPbBr_3$-Au nanocrystal suspensions (spectra b-f), (A) kept in dark and (B) with steady state white light irradiation (100 mW/cm^2). The concentration of Au in $CsPbBr_3$ –Au was 12 μM. Spectrum 'a' corresponds to pristine $CsPbBr_3$ sample. Spectra b-f were recorded at different time intervals. (C) Photoluminescence (intensity monitored at 510 nm) recovery during 30 min irradiation (red squares) and dark (black circles) of $CsPbBr_3$-Au nanocrystal suspensions in toluene. The photoluminescence of pristine $CsPbBr_3$ prior to Au modification is shown as a reference.

during this process. We also checked the emission recovery for $CsPbBr_3$-Au samples with different (1.6μM-12μM) Au concentrations (see SI Figures S5-S8). In all these cases, we observed a recovery of the photoluminescence (99%-85%) following steady state illumination.

The photoluminescence decay and transient bleach recovery in the transient absorption measurements are compared in Figure 5. The time resolved transient absorption spectra of photoirradiated $CsPbBr_3$ –Au sample is shown in Figure S9. The decay profiles for photoluminescence and bleach recovery of the photoirradiated $CsPbBr_3$-Au sample matched that of the original $CsPbBr_3$ sample (i.e., without modification with gold). These results suggest that the interaction between the Au nanoparticles and the

$CsPbBr_3$ nanocrystals has been greatly reduced following steady state irradiation with light. It is thus interesting to find out the reason behind the weakened interaction between $CsPbBr_3$ and Au following the photoirradiation in $CsPbBr_3$ –Au nanocrystals.

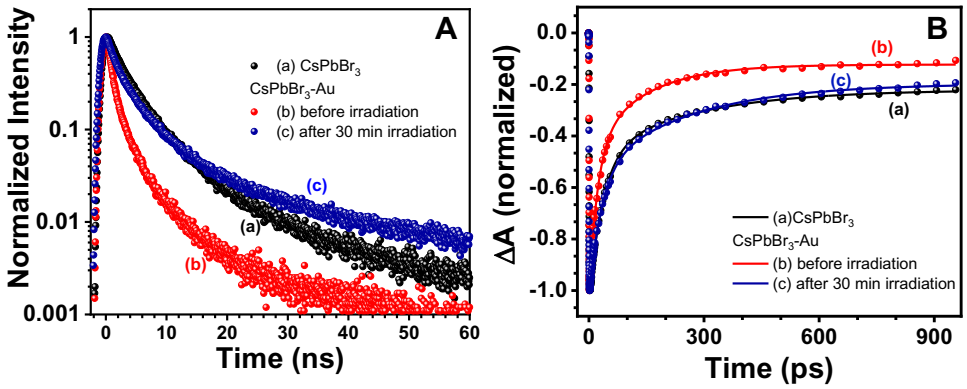

Figure 5. (A) Photoluminescence (PL) decay monitored at 510 nm, of (a) $CsPbBr_3$ nanocrystals and (b,c) $CsPbBr_3$-Au heterostructures in toluene:(b) before and (c) after 30 min of irradiation. (B) Recovery of the transient bleach signal recorded at the bleach maximum, 510 nm for (a) $CsPbBr_3$ nanocrystals and (b,c) $CsPbBr_3$-Au heterostructure suspensions: (b) before and (c) after 30 min of irradiation. Excitation was at 370 nm for PL decay and 400 nm for transient absorption measurements.

Expulsion of Gold nanoparticles from $CsPbBr_3$-Au Heterostructures. We sampled the $CsPbBr_3$-Au nanocrystal suspension at different photoirradiation times and carried out TEM analysis. The images recorded at four different times are shown in Figure 6. Before irradiation, the gold particles are well distributed and attached to individual $CsPbBr_3$ nanocrystallites. Once they are subjected to photoirradiation the particles become detached (Figure 6B). At 30 minutes these small nanoparticles seem to form a network of clusters. The background image of $CsPbBr_3$ nanoparticles show cleaner $CsPbBr_3$ surfaces. With continued photoirradiation the gold clusters grow into larger size Au nanoparticles (20-100 nm diameter). These results indicate that the gold nanoparticles are no longer attached to $CsPbBr_3$ nanoparticles after irradiation, thus, reducing the interaction and restoring the characteristics of pristine $CsPbBr_3$ nanoparticles.

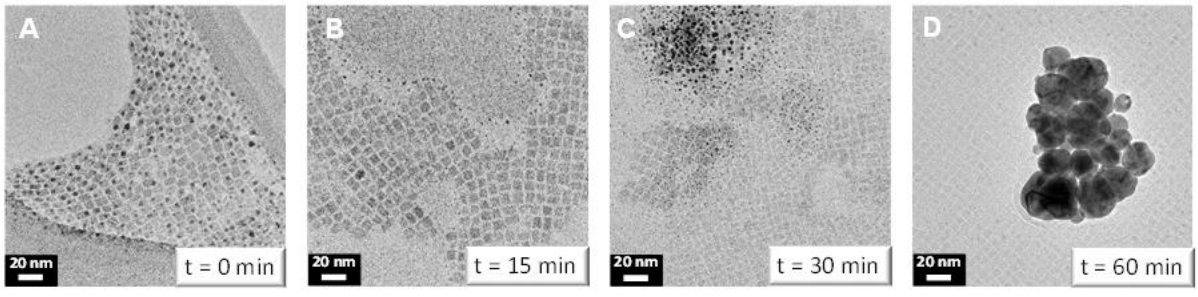

Figure 6: TEM images of Au-$CsPbBr_3$ nanocrystal samples following photoirradiation (white light, 100 mW/cm^2) at times, (A) 0 min, (B) 15 min, (C) 30 min, and (D) 60 min respectively.

Semiconductor-metal heterostructures have been widely used in photocatalysis. For example, noble or precious metals deposited on a semiconductor serve as a co-catalyst to promote reduction reaction (e.g., H_2 generation in a water splitting process).[60-62] The metal particles capture electrons from the semiconductor and shuttle electrons between the semiconductor and the redox species by lowering the overpotential needed for the reduction. In the majority of these examples the anchoring of the metal particles on the semiconductor surface remains intact even during extended periods of photoirradiation. The results described in Figures 4-6 however show an unusual photo-effect of expulsion of gold nanoparticles from $CsPbBr_3$-Au heterostructures. The transient absorption data shows clear evidence of photo-induced electron transfer from the $CsPbBr_3$ to the Au in the $CsPbBr_3$-Au heterostructures. Thus, a

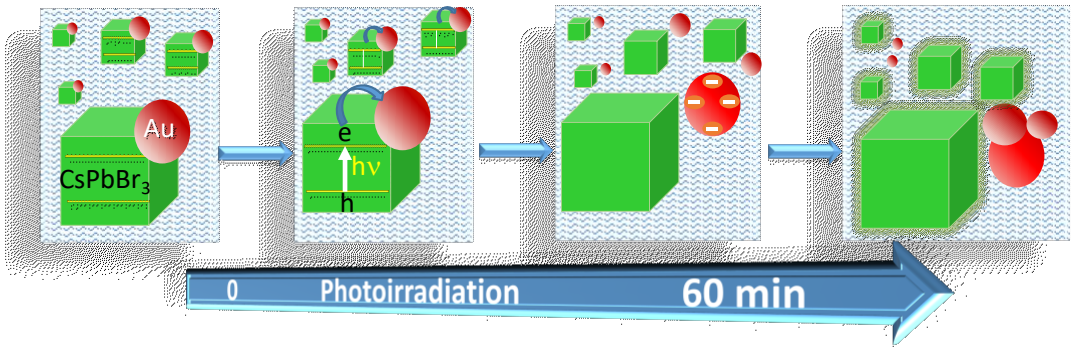

Scheme 2. Photoinduced electron transfer from excited $CsPbBr_3$ into Au nanoparticles followed by repulsion of charged Au nanoparticles during steady state irradiation of $CsPbBr_3$-Au heterostructures suspended in toluene.

possible explanation for expulsion of the gold nanoparticles from the heterostructures during steady-state illumination could be charging of gold nanoparticles, which makes them unstable.

The photoinduced events of $CsPbBr_3$-Au heterostructures are illustrated in Scheme 2. As shown earlier, smaller gold nanoparticles are efficient in capturing and storing photogenerated electrons from the semiconductor.[63,64] The storage of electrons in such small metal nanoparticles has been shown by monitoring quantized capacitance,[14,65] blue-shift in plasmon absorption[16-18] and on-demand electron transfer at delayed time interval.[64] We expect similar electron capture by Au nanoparticles, which causes charging during photoirradiation and subsequent detachment from the $CsPbBr_3$ surface. Both the emission recovery and the TEM images support the steps involved in the expulsion of gold nanoparticles during photoirradiation.

Concluding Remarks

A stable design of perovskite-metal heterostructures remains a challenge. Unlike metal chalcogenide or metal oxide semiconductors, the surface of perovskite nanocrystals is susceptible to environmental changes. The Au nanocrystals formed through the reduction by oleylamine ligand are loosely bound to the semiconductor surface. These nonplasmonic (small size of ~1nm) nanoparticles accept electrons from the perovskite particles to become charged and (eventually) be expelled during steady state photoirradiation. Ultrafast measurements show that electron transfer to Au occurs from both hot and band edge electrons in the $CsPbBr_3$ conduction band, with rate constants of $(2.43 \pm 0.39)\times10^{12}$ s^{-1} and $(1.73 \pm 0.27)\times10^{10}$ s^{-1}, respectively. The charged gold particles are then repelled from the negatively charged

CsPpbBr3 surface, thus necessitating a stronger linkage between the two. The use of a bifunctional molecular bridge to establish a stronger linkage between the semiconductor and metal nanoparticles (e.g., mercaptopropionic acid employed to link TiO_2 and Au nanoparticles[64]) is needed to develop a stable heterostructures.

Acknowledgement

The research described herein is supported by the Division of Chemical Sciences, Geosciences, and Biosciences, Office of Basic Energy Sciences of the U.S. Department of Energy, through award (award DE-FC02- 04ER15533. GVH acknowledges support of the National Science Foundation through Grant CHE-2002300. We also acknowledge the University of Notre Dame Equipment Restoration and Renewal (ERR) program for the purchase of the Spectra Physics laser used for the transient absorption measurements. We would like to thank Subila Balakrishnan for conducting preliminary experiments. This is contribution number NDRL No. 5323 from the Notre Dame Radiation Laboratory.

Supporting Information The supporting information include control experiments, histogram analysis, emission spectra and transient absorption measurements at different Au concentrations. The Supporting Information is available free of charge at https://pubs.acs.org/doi/10.1021/XXXX

References

(1) Kamat, P. V. Photophysical, Photochemical and Photocatalytic Aspects of Metal Nanoparticles, *J. Phys. Chem. B* **2002,** *106*, 7729-7744.
(2) Zhang, Z.; Yates, J. T. Band Bending in Semiconductors: Chemical and Physical Consequences at Surfaces and Interfaces, *Chemical Reviews* **2012,** *112*, 5520-5551.
(3) Dutta, S. K.; Mehetor, S. K.; Pradhan, N. Metal Semiconductor Heterostructures for Photocatalytic Conversion of Light Energy, *The Journal of Physical Chemistry Letters* **2015,** *6*, 936-944.
(4) Subramanian, V.; Wolf, E.; Kamat, P. V. Semiconductor-Metal Composite Nanostructures. To What Extent Metal Nanoparticles (Au, Pt, Ir) Improve the Photocatalytic Activity of TiO_2 Films?, *J. Phys. Chem. B* **2001,** *105*, 11439-11446.
(5) Christopher, P.; Xin, H.; Linic, S. Visible-Light-Enhanced Catalytic Oxidation Reactions on Plasmonic Silver Nanostructures, *Nature Chemistry* **2011,** *3*, 467-472.
(6) Faucheaux, J. A.; Stanton, A. L. D.; Jain, P. K. Plasmon Resonances of Semiconductor Nanocrystals: Physical Principles and New Opportunities, *The Journal of Physical Chemistry Letters* **2014,** *5*, 976-985.
(7) Govorov, A. O.; Zhang, H.; Gun'ko, Y. K. Theory of Photoinjection of Hot Plasmonic Carriers from Metal Nanostructures into Semiconductors and Surface Molecules, *The Journal of Physical Chemistry C* **2013,** *117*, 16616-16631.
(8) Hartland, G. V.; Besteiro, L. V.; Johns, P.; Govorov, A. O. What's so Hot about Electrons in Metal Nanoparticles?, *ACS Energy Letters* **2017**, 1641-1653.
(9) Mohan, V.; Wu, E.; Heo, J.; Das, A.; Jain, P. K. Synergistic Photochemistry of Alcohols Catalyzed by Plasmonic Nanoparticles and a Metal Complex, *ACS Energy Letters* **2021,** *6*, 1980-1989.
(10) Yu, S.; Wilson, A. J.; Kumari, G.; Zhang, X.; Jain, P. K. Opportunities and Challenges of Solar-Energy-Driven Carbon Dioxide to Fuel Conversion with Plasmonic Catalysts, *ACS Energy Letters* **2017,** *2*, 2058-2070.
(11) Cushing, S. K.; Wu, N. Progress and Perspectives of Plasmon-Enhanced Solar Energy Conversion, *The Journal of Physical Chemistry Letters* **2016,** *7*, 666-675.
(12) Wu, K.; Chen, J.; McBride, J. R.; Lian, T. Efficient Hot-Electron Transfer by a Plasmon-Induced Interfacial Charge-Transfer Transition, *Science* **2015,** *349*, 632-635.
(13) Huang, X.; Li, H.; Zhang, C.; Tan, S.; Chen, Z.; Chen, L.; Lu, Z.; Wang, X.; Xiao, M. Efficient plasmon-hot electron conversion in Ag–CsPbBr3 hybrid nanocrystals, *Nature Communications* **2019,** *10*, 1163.
(14) Chen, S.; Ingram, R. S.; Hostetler, M. J.; Pietron, J. J.; Murray, R. W.; Schaaff, T. G.; Khoury, J. T.; Alvarez, M. M.; Whetten, R. L. Gold Nanoelectrodes of Varied Size: Transition to Molecule-Like Charging, *Science* **1998,** *280*, 2098-2101.
(15) Chen, S.; Murray, R. W. Electrochemical Quantized Capacitance Charging of Surface Ensembles of Gold Nanoparticles, *J. Phys. Chem. B* **1999,** *103*, 9996 -10000.
(16) Hirakawa, T.; Kamat, P. V. Charge Separation and Catalytic Activity of Ag@TiO_2 Core-Shell Composite Clusters under UV-Irradiation, *J. Am. Chem. Soc.* **2005,** *127*, 3928-3934.
(17) Takai, A.; Kamat, P. V. Capture, Store and Discharge. Shuttling Photogenerated Electrons Across TiO_2-Silver Interface, *ACS Nano* **2011,** *4*, 7369–7376.
(18) Choi, H.; Chena, W. T.; Kamat, P. V. Know Thy Nano Neighbor. Plasmonic *versus* Electron Charging Effects of Gold Nanoparticles in Dye Sensitized Solar Cells, *ACS Nano* **2012,** *6*, 4418–4427.
(19) Shyamal, S.; Pradhan, N. Halide Perovskite Nanocrystal Photocatalysts for CO_2 Reduction: Successes and Challenges, *The Journal of Physical Chemistry Letters* **2020,** *11*, 6921-6934.
(20) Huang, H.; Pradhan, B.; Hofkens, J.; Roeffaers, M. B. J.; Steele, J. A. Solar-Driven Metal Halide Perovskite Photocatalysis: Design, Stability, and Performance, *ACS Energy Letters* **2020,** *5*, 1107-1123.

(21) Shamsi, J.; Urban, A. S.; Imran, M.; De Trizio, L.; Manna, L. Metal Halide Perovskite Nanocrystals: Synthesis, Post-Synthesis Modifications, and Their Optical Properties, *Chemical Reviews* **2019,** *119*, 3296-3348.
(22) Rahmany, S.; Etgar, L. Semitransparent Perovskite Solar Cells, *ACS Energy Letters* **2020,** *5*, 1519-1531.
(23) Chen, J.; Park, N.-G. Materials and Methods for Interface Engineering toward Stable and Efficient Perovskite Solar Cells, *ACS Energy Letters* **2020,** *5*, 2742-2786.
(24) Li, M.; Li, H.; Fu, J.; Liang, T.; Ma, W. Recent Progress on the Stability of Perovskite Solar Cells in a Humid Environment, *The Journal of Physical Chemistry C* **2020,** *124*, 27251-27266.
(25) Manekkathodi, A., et al. Solution-Processed Perovskite-Colloidal Quantum Dot Tandem Solar Cells for Photon Collection Beyond 1000 Nm, *Journal of Materials Chemistry A* **2019,** *7*, 26020-26028.
(26) Wang, X.; Bao, Z.; Chang, Y.-C.; Liu, R.-S. Perovskite Quantum Dots for Application in High Color Gamut Backlighting Display of Light-Emitting Diodes, *ACS Energy Letters* **2020**, 3374-3396.
(27) Wei, Y.; Cheng, Z.; Lin, J. An Overview on Enhancing the Stability of Lead Halide Perovskite Quantum Dots and Their Applications in Phosphor-Converted LEDs, *Chemical Society Reviews* **2019,** *48*, 310-350.
(28) Rybin, N., et al. Effects of Chlorine Mixing on Optoelectronics, Ion Migration, and Gamma-Ray Detection in Bromide Perovskites, *Chemistry of Materials* **2020,** *32*, 1854-1863.
(29) He, Y.; Stoumpos, C. C.; Hadar, I.; Luo, Z.; McCall, K. M.; Liu, Z.; Chung, D. Y.; Wessels, B. W.; Kanatzidis, M. G. Demonstration of Energy-Resolved γ-Ray Detection at Room Temperature by the $CsPbCl_3$ Perovskite Semiconductor, *Journal of the American Chemical Society* **2021,** *143*, 2068-2077.
(30) Wei, H. T., et al. Sensitive X-Ray Detectors Made of Methylammonium Lead Tribromide Perovskite Single Crystals, *Nature Photonics* **2016,** *10*, 333-+.
(31) Clinckemalie, L.; Valli, D.; Roeffaers, M. B. J.; Hofkens, J.; Pradhan, B.; Debroye, E. Challenges and Opportunities for CsPbBr3 Perovskites in Low- and High-Energy Radiation Detection, *ACS Energy Letters* **2021,** *6*, 1290-1314.
(32) Wu, R. S., et al. Prominent Efficiency Enhancement in Perovskite Solar Cells Employing Silica-Coated Gold Nanorods, *Journal of Physical Chemistry C* **2016,** *120*, 6996-7004.
(33) Carretero-Palacios, S.; Calvo, M. E.; Miguez, H. Absorption Enhancement in Organic-Inorganic Halide Perovskite Films with Embedded Plasmonic Gold Nanoparticles, *Journal of Physical Chemistry C* **2015,** *119*, 18635-18640.
(34) Huang, X. Y.; Li, H. B.; Zhang, C. F.; Tan, S. J.; Chen, Z. Z.; Chen, L.; Lu, Z. D.; Wang, X. Y.; Xiao, M. Efficient plasmon-hot electron conversion in Ag-CsPbBr3 hybrid nanocrystals, *Nature Communications* **2019,** *10*.
(35) Shlenskaya, N. N.; Belich, N. A.; Gratzel, M.; Goodilin, E. A.; Tarasov, A. B. Light-Induced Reactivity of Gold And Hybrid Perovskite as a New Possible Degradation Mechanism in Perovskite Solar Cells, *Journal of Materials Chemistry A* **2018,** *6*, 1780-1786.
(36) Kerner, R. A.; Schulz, P.; Christians, J. A.; Dunfield, S. P.; Dou, B. J.; Zhao, L. F.; Teeter, G.; Berry, J. J.; Rand, B. P. Reactions at Noble Metal Contacts with Methylammonium Lead Triiodide Perovskites: Role of Underpotential Deposition and Electrochemistry, *Apl Materials* **2019,** *7*.
(37) Ravi, V. K.; Saikia, S.; Yadav, S.; Nawale, V. V.; Nag, A. $CsPbBr_3$/ZnS Core/Shell Type Nanocrystals for Enhancing Luminescence Lifetime and Water Stability, *ACS Energy Letters* **2020,** *5*, 1794-1796.
(38) Shi, J.; Ge, W.; Zhu, J.; Saruyama, M.; Teranishi, T. Core–Shell $CsPbBr_3$@CdS Quantum Dots with Enhanced Stability and Photoluminescence Quantum Yields for Optoelectronic Devices, *ACS Applied Nano Materials* **2020,** *3*, 7563-7571.
(39) Balakrishnan, S. K.; Kamat, P. V. Au–$CsPbBr_3$ Hybrid Architecture: Anchoring Gold Nanoparticles on Cubic Perovskite Nanocrystals, *ACS Energy Letters* **2017**, 88-93.

(40) Roman, B. J.; Otto, J.; Galik, C.; Downing, R.; Sheldon, M. Au Exchange or Au Deposition: Dual Reaction Pathways in Au–CsPbBr3 Heterostructure Nanoparticles, *Nano Letters* **2017,** *17*, 5561-5566.
(41) Protesescu, L.; Yakunin, S.; Bodnarchuk, M. I.; Krieg, F.; Caputo, R.; Hendon, C. H.; Yang, R. X.; Walsh, A.; Kovalenko, M. V. Nanocrystals of Cesium Lead Halide Perovskites ($CsPbX_3$, X = Cl, Br, and I): Novel Optoelectronic Materials Showing Bright Emission with Wide Color Gamut, *Nano Letters* **2015,** *15*, 3692-3696.
(42) Balakrishnan, S. K.; Kamat, P. V. Ligand Assisted Transformation of Cubic $CsPbBr_3$ Nanocrystals into Two-Dimensional $CsPb_2Br_5$ Nanosheets, *Chemistry of Materials* **2018,** *30*, 74–78.
(43) Mondal, N.; De, A.; Samanta, A. Achieving Near-Unity Photoluminescence Efficiency for Blue-Violet-Emitting Perovskite Nanocrystals, *ACS Energy Letters* **2019,** *4*, 32-39.
(44) Costi, R.; Saunders, A. E.; Elmalem, E.; Salant, A.; Banin, U. Visible Light-Induced Charge Retention and Photocatalysis with Hybrid CdSe-Au Nanodumbbells, *Nano Letters* **2008,** *8*, 637-641.
(45) Gooding, A. K.; Gomez, D. E.; Mulvaney, P. The Effects of Electron and Hole Injection on the Photoluminescence of CdSe/CdS/ZnS Nanocrystal Monolayers, *ACS Nano* **2008,** *2*, 669-676.
(46) Pons, T.; Medintz, I. L.; Sapsford, K. E.; Higashiya, S.; Grimes, A. F.; English, D. S.; Mattoussi, H. On the Quenching of Semiconductor Quantum Dot Photoluminescence by Proximal Gold Nanoparticles, *Nano Lett.* **2007,** *7*, 3157-3164.
(47) Klimov, V. I. Optical Nonlinearities and Ultrafast Carrier Dynamics in Semiconductor Nanocrystals, *J. Phys. Chem. B* **2000,** *104*, 6112 - 6123.
(48) Kamat, P. V.; Dimitrijevic, N. M.; Nozik, A. J. Dynamic Burstein-Moss shift in semiconductor colloids, *J. Phys. Chem.* **1989,** *93*, 2873-5.
(49) Harris, C.; Kamat, P. V. Photocatalytic Events of CdSe Quantum Dots in Confined Media. Electrodic Behavior of Coupled Platinum Nanoparticles, *ACS Nano* **2010,** *4*, 7321–7330.
(50) Li, M.; Cushing, S. K.; Wang, Q.; Shi, X.; Hornak, L. A.; Hong, Z.; Wu, N. Size-Dependent Energy Transfer between CdSe/ZnS Quantum Dots and Gold Nanoparticles, *The Journal of Physical Chemistry Letters* **2011,** *2*, 2125-2129.
(51) Wu, K. F.; Zhu, H. M.; Liu, Z.; Rodriguez-Cordoba, W.; Lian, T. Q. Ultrafast Charge Separation and Long-Lived Charge Separated State in Photocatalytic CdS-Pt Nanorod Heterostructures, *Journal of the American Chemical Society* **2012,** *134*, 10337-10340.
(52) Yu, P.; Wen, X.; Lee, Y.-C.; Lee, W.-C.; Kang, C.-C.; Tang, J. Photoinduced ultrafast charge separation in plexcitonic CdSe/Au and CdSe/Pt nanorods, *The Journal of Physical Chemistry Letters* **2013,** *4*, 3596-3601.
(53) Okuhata, T.; Katayama, T.; Tamai, N. Ultrafast and hot electron transfer in CdSe QD–Au hybrid nanostructures, *The Journal of Physical Chemistry C* **2019,** *124*, 1099-1107.
(54) Liu, Y.; Chen, Q.; Cullen, D. A.; Xie, Z.; Lian, T. Efficient hot electron transfer from small Au nanoparticles, *Nano letters* **2020,** *20*, 4322-4329.
(55) Camargo, F. V.; Ben-Shahar, Y.; Nagahara, T.; Panfil, Y. E.; Russo, M.; Banin, U.; Cerullo, G. Visualizing Ultrafast Electron Transfer Processes in Semiconductor–Metal Hybrid Nanoparticles: Toward Excitonic–Plasmonic Light Harvesting, *Nano letters* **2021,** *21*, 1461-1468.
(56) DuBose, J. T.; Kamat, P. V. Probing Perovskite Photocatalysis. Interfacial Electron Transfer between $CsPbBr_3$ and Ferrocene Redox Couple, *The Journal of Physical Chemistry Letters* **2019,** *10*, 6074-6080.
(57) Kobosko, S. M.; DuBose, J. T.; Kamat, P. V. Perovskite Photocatalysis. Methyl Viologen Induces Unusually Long-Lived Charge Carrier Separation in $CsPbBr_3$ Nanocrystals, *ACS Energy Letters* **2020,** *5*, 221-223.
(58) Li, Q.; Lian, T. Ultrafast Charge Separation in Two-Dimensional $CsPbBr_3$ Perovskite Nanoplatelets, *The Journal of Physical Chemistry Letters* **2019,** *10*, 566-573.

(59) Schanze, K. S.; Kamat, P. V.; Yang, P.; Bisquert, J. Progress in Perovskite Photocatalysis, *ACS Energy Letters* **2020,** *5*, 2602-2604.
(60) Hansen, J. N.; Prats, H.; Toudahl, K. K.; Mørch Secher, N.; Chan, K.; Kibsgaard, J.; Chorkendorff, I. Is There Anything Better than Pt for HER?, *ACS Energy Letters* **2021,** *6*, 1175-1180.
(61) Maeda, K.; Domen, K. Photocatalytic Water Splitting: Recent Progress and Future Challenges, *The Journal of Physical Chemistry Letters* **2010,** *1*, 2655-2661.
(62) Pinaud, B. A., et al. Technical and Economic Feasibility of Centralized Facilities for Solar Hydrogen Production *via* Photocatalysis and Photoelectrochemistry, *Energy & Environmental Science* **2013,** *6*, 1983-2002.
(63) Redmond, P. L.; Brus, L. E. "Hot Electron" Photo-Charging and Electrochemical Discharge Kinetics of Silver Nanocrystals, *The Journal of Physical Chemistry C* **2007,** *111*, 14849-14854.
(64) Subramanian, V.; Wolf, E. E.; Kamat, P. V. Catalysis with TiO_2/Au Nanocomposites. Effect of Metal Particle Size on the Fermi Level Equilibration, *J. Am. Chem. Soc.* **2004,** *126*, 4943-4950.
(65) Hicks, J. F.; Templeton, A. C.; Chen, S.; Sheran, K. M.; Jasti, R.; Murray, R. W.; Debord, J.; Schaaff, T. G.; Whetten, R. L. The Monolayer Thickness Dependence of Quantized Double-Layer Capacitances of Monolayer-Protected Gold Clusters, *Anal. Chem.* **1999,** *71*, 3703 -3711.